

Adaptive solution to the Poisson equation with the Symmetric Interior Penalty discontinuous Galerkin method on the L-shaped domain

Simone Appella, Chris Budd and Tristan Pryer

April 23, 2021

1 Introduction

Solutions of elliptic boundary value problems defined on non-convex domains have singular behaviour near re-entrant corners. This occurs even when data of the underlying problem are very smooth. Such singular behaviour affects the accuracy of Finite Element Methods (FEMs) throughout the whole domain. Hence, the solutions of the corresponding problems are typically only in H^k for small $k > 1$ [BG88; BG89]. A theoretical mathematical framework able to describe such singular behaviour is given by the theory of weighted Sobolev spaces, which were originally studied in [BR72; BKP79] for elasticity and potential problems.

In this chapter, we treat the Poisson equation defined on the L-shaped domain with prescribed Dirichlet boundary conditions. The numerical solution of the Poisson equation on non-convex domains has been already addressed in [ZSG02; SH16; ZS02]. The spatial discretisation is performed with the discontinuous Galerkin (dG) method, introduced in [RH73] for neutron transport problems. The method has been then extended to solve first order hyperbolic systems and to general convection-diffusion problems [CC98; CC01].

The popularity of the dG method resides in its flexibility with respect to adapted elements of various types and shapes. There exist several possibilities to formulate dG schemes for this class of problems: either resorting to an interior penalty method [Arn82; Arn+00; Arn+02], or omitting stabilization completely [Ric92]. In all these works, error estimates of h - or p -type under strong regularity assumptions are given. In order to resolve the singularities numerically with the *Symmetric Interior Penalty* (SIP) dG method, appropriate adaptive mesh strategies must be carefully selected to obtain the optimal order of convergence. Our research is inspired by the work of [Wih03; Sch98].

The main contribution of our work consists in the derivation of an *a-posteriori* estimate in the L^2 norm for the SIP-dG method and its application for different h - and r -adaptive mesh strategies. The derivation of the a-posteriori estimate is based on the following steps:

- State the Poisson problem with non-homogeneous Dirichlet and/or Neumann boundary conditions. Claim existence and uniqueness of the solution using the framework of the weighted Sobolev spaces.
- Define the SIP-dG variational formulation of the Poisson problem.
- State consistency of the SIP-dG method and the resulting Galerkin orthogonality with respect to the dG space.

- Formulate the weak dual problem of the Poisson equation with the error as given datum and derive the corresponding SIP-dG variational formulation.
- Define a proper interpolant of the solution of the dual problem and exploit the Galerkin orthogonality, interpolation bounds, and regularity results [BG88] to obtain the a-posteriori estimate.

In §4, the adapted SIP-dG method will be tested on the Poisson equation for different adaptive strategies. The rate of convergence in the L^2 norm will be first computed using the h -refinement, with the local error estimator based on the a-posteriori bound. As r -adaptive methods, Winslow's Moving Mesh PDE (MMPDE) and an Optimal Transport (OT) strategy will be employed. The comparison between h - and r -adaptive methods will be performed in terms of accuracy and quality of the resulting meshes. We will show that all those strategies derived from the a-posteriori estimate and the OT mesh yields optimal order of convergence.

We will draw our conclusions and propose ideas to further expand this work in §6.

2 Problem setup and discretisation

Let $\Omega \subset \mathbb{R}^2$ be a bounded, polygonal domain with outward unit normal \vec{n}_Ω . Suppose that the boundary $\Gamma = \partial\Omega$ is composed by a Dirichlet part Γ_D with $|\Gamma_D| > 0$ and a Neumann part Γ_N such that:

$$\bar{\Gamma} = \bar{\Gamma}_D \cup \bar{\Gamma}_N. \quad (1)$$

All the vertices are included in the closure. The corner vertices and the points of changing boundary conditions are *singular points* and collected in the set

$$SP(\Omega, \Gamma_D, \Gamma_N) = \{A_i : i = 1, \dots, M\}. \quad (2)$$

The interior opening angle of the domain at A_i is measured anti-clockwise and denoted by $\omega \in (0, 2\pi]$. The case $\omega = \pi$ allows boundary conditions to switch from Neumann to Dirichlet or vice versa.

To account for the regularity of the elliptic problem, suitable Sobolev spaces will be introduced. A weight $\vec{\beta}_i \in (0, 1]$ is associated with each singular point $A_i \in SP(\Omega, \Gamma_D, \Gamma_N)$ and stored in the vector $\vec{\beta} = (\beta_1, \dots, \beta_M)$. For any number $k \in \mathbb{R}$, we let

$$\vec{\beta} + k = (\beta_1 + k, \dots, \beta_M + k).$$

We then introduce the weight function on Ω :

$$\Phi_{\vec{\beta}}(\vec{x}) = \prod_{i=1}^M r_i(\vec{x})^{\beta_i}, \quad r_i(\vec{x}) = |\vec{x} - A_i|.$$

Then, for any integers $m \geq l \geq 0$, the weighted Sobolev spaces $H_{\vec{\beta}}^{m,l}(\Omega)$ are defined as completion of the space $C^\infty(\bar{\Omega})$ with respect to the weighted Sobolev norms

$$\begin{aligned} \|u\|_{H_{\vec{\beta}}^{m,l}(\Omega)}^2 &= \|u\|_{H^{l-1}(\Omega)}^2 + |u|_{H_{\vec{\beta}}^{m,l}(\Omega)}^2, \quad l \geq 1 \\ \|u\|_{H_{\vec{\beta}}^m(\Omega)}^2 &= \sum_{|\alpha|=k}^m \left\| |D^\alpha u| \Phi_{\vec{\beta}+k} \right\|_{L^2(\Omega)}^2, \quad l = 0, \end{aligned} \quad (3)$$

where

$$|u|_{H_{\vec{\beta}}^{m,l}(\Omega)}^2 = \sum_{\substack{|\alpha|=k \\ k=l}}^m \left\| |D^\alpha u| \Phi_{\vec{\beta}+k-l} \right\|_{L^2(\Omega)}^2$$

and

$$D^\alpha u = \frac{\partial^{|\alpha|} u}{\partial x_1^{\alpha_1} \partial x_2^{\alpha_2}},$$

with $\alpha = (\alpha_1, \alpha_2) \in \mathbb{N}^2$ and $|\alpha| = \alpha_1 + \alpha_2$.

Fractional Sobolev spaces for $m \in \mathbb{R}$ appear naturally as the correct range of the continuous trace map

$$\tau : H^m(\Omega) \rightarrow H^{m-1/2}(\Gamma), \quad m > 1/2,$$

and will be used to define properly the boundary conditions for the Poisson problem.

We mention the following remark proved in [Wih03]:

Remark 1 (Properties of the weighted Sobolev spaces [Wih03, Remark 1.2.2]) *The following properties hold:*

1. If $u \in H_{\vec{\beta}}^{m,m}(\Omega)$, $m \geq 0$, then $u \in H^m(\Omega_0)$ for all domains $\Omega_0 \subset \Omega$ with

$$P \notin \overline{\Omega_0} \quad \forall P \in SP(\Omega, \Gamma_D, \Gamma_N).$$

2. Although $H_{\vec{\beta}}^{2,2}(\Omega) \not\subset H^2(\Omega)$, it was proven in [BKP79] that $H_{\vec{\beta}}^{2,2}(\Omega) \subset C^0(\overline{\Omega})$.

3. For $u \in H_{\vec{\beta}}^{2,2}(\Omega)$, there holds $\nabla u \in H_{\vec{\beta}}^{1,1}(\Omega)^2$.

2.1 Poisson equation in 2D

Let $\Omega \subset \mathbb{R}^2$ be a bounded, polygonal domain. Consider the following *Poisson problem*

$$\begin{aligned} -\Delta u &= f \text{ in } \Omega \\ u &= u_D \text{ on } \Gamma_D \\ \nabla u \cdot \vec{n}_\Omega &= g \text{ on } \Gamma_N. \end{aligned} \tag{4}$$

Here, f is a given datum lying on the dual space of $H_0^1(\Omega)$ and denoted by $H^{-1}(\Omega)$, $u_D \in H^{1/2}(\Gamma_D)$ and $g \in H^{-1/2}(\Gamma_N)$ are prescribed Dirichlet and Neumann boundary conditions, respectively. In the framework of weighted Sobolev spaces, the existence and uniqueness of problem (4) is stated in the following Theorem:

Theorem 2 (Regularity of the Poisson equation [BG88, Theorem 3.1]) *Let Ω be a polygon in \mathbb{R}^2 and $m \geq 0$ a given integer. Then, there exists a weight vector $\vec{\beta}_{min}$ with $0 \leq \vec{\beta}_{min} < 1$ depending on the opening angles at the vertices $A_i \in SP(\Omega, \Gamma_D, \Gamma_N)$, such that for weight vectors $\vec{\beta}$ with $\vec{\beta}_{min} \leq \vec{\beta} < 1$ and for*

$$f \in H_{\vec{\beta}}^{m,0}(\Omega), \quad u_D \in H_{\vec{\beta}}^{m+3/2,3/2}(\Gamma_D), \quad g \in H_{\vec{\beta}}^{m+1/2,1/2}(\Gamma_N),$$

the problem (4) has a unique solution $u \in H_{\vec{\beta}}^{m+2,2}(\Omega)$.

Remark 3 ([BG88, Theorem 2.1 - Remark 3]) In the case of the Poisson equation the value of $\vec{\beta}_{min}$ is well-known at each corner A_i and given by

$$\beta_{min,i} = \begin{cases} 1 - \frac{\pi}{\omega} & \text{if } \overline{A_i A_{i+1}} \in \Gamma_D \text{ or } \Gamma_N, \\ 1 - \frac{\pi}{2\omega} & \text{otherwise.} \end{cases} \quad (5)$$

2.2 Finite element spaces

Let \mathcal{T} be a conforming mesh of Ω into simplicial open elements K :

$$\mathcal{T} = \{K_i\}_i, \quad \bigcup_{K \in \mathcal{T}} \overline{K} = \overline{\Omega}.$$

We consider \mathcal{T} is a finite family of sets such that:

1. $K \in \mathcal{T}$ implies K is an open triangle or quadrilateral,
2. for any $K, J \in \mathcal{T}$ we have that $\overline{K} \cap \overline{J}$ is either empty or a complete $(2-r)$ -dimensional simplex/box (i.e., it is either a vertex for $r=2$, or an edge for $r=1$, or the whole of \overline{K} and \overline{J}) of both \overline{K} and \overline{J} ,
3. $\bigcup_{K \in \mathcal{T}} \overline{K} = \overline{\Omega}$.

Additionally, for each $K \in \mathcal{T}$ we introduce

$$h_K = \text{diam}(K) := \sup_{x,y \in K} |x - y|$$

and

$$\rho_K = \sup\{\text{diam}(B) : B \text{ is an open ball contained in } K\}.$$

Finally, the *mesh width* of \mathcal{T} is given by

$$h_{\mathcal{T}} = \max_{K \in \mathcal{T}} h_K.$$

We will also assume that all the meshes generated by the h - r -refinement are *shape regular*. Let $\mathcal{G} = \{\mathcal{T}_i\}_{i \in \mathbb{N}}$ be a family of meshes, then \mathcal{G} is characterised by the shape regularity $\mu(\mathcal{T})$ if

$$\mu(\mathcal{T}) = \min_{K \in \mathcal{T}_i} \frac{h_K}{\rho_K} > 0, \quad \forall i \in \mathbb{N}, \quad (6)$$

The set of all edges of \mathcal{T} is denoted by \mathcal{E} , which we partition into subsets $\mathcal{E}_D, \mathcal{E}_N, \mathcal{E}_I$, consisting of edges lying on the Dirichlet boundary Γ_D , the Neumann boundary Γ_N , and the interior edges, respectively. The corresponding quantities for each individual element K are denoted by $\mathcal{E}(K), \mathcal{E}_D(K), \mathcal{E}_N(K), \mathcal{E}_I(K)$, respectively.

We split the index set $\{1, \dots, M\}$ of boundary edges e_i into \mathcal{D} and \mathcal{N} , on which Dirichlet and Neumann boundary conditions are applied, respectively. This leads to $\overline{\Gamma}_D = \bigcup_{i \in \mathcal{D}} \overline{e}_i$ and $\overline{\Gamma}_N = \bigcup_{i \in \mathcal{N}} \overline{e}_i$.

We define the *finite element space*

$$\mathbb{V} := \{v \in L^2(\Omega) : v|_K \in \mathbb{P}^p(K) \quad \forall K \in \mathcal{T}\}, \quad (7)$$

where $\mathbb{P}^p(K)$ is the space of polynomials of total degree p .

We remark that the space \mathbb{V} does not carry any inter-element continuity and does not encode any boundary condition. These will be enforced weakly in the variational scheme. Given an edge γ of \mathcal{T} , we define the jump and average operator of $v \in \mathbb{V}$ on the edges \mathcal{E} at $\vec{x} \in \gamma$ by

$$[\![v]\!] := \begin{cases} v|_K \vec{n}_K + v|_{K'} \vec{n}_{K'} & \text{on } \gamma = \partial K \cap \partial K' \\ v|_K \vec{n}_\Omega & \text{on } \gamma = \partial K \cap \Gamma_D \end{cases} \quad [\![\vec{v}]\!] := \begin{cases} \vec{v}|_K \cdot \vec{n}_K + \vec{v}|_{K'} \cdot \vec{n}_{K'} & \text{on } \gamma = \partial K \cap \partial K' \\ \vec{v}|_K \cdot \vec{n}_\Omega & \text{on } \gamma = \partial K \cap \Gamma_D \end{cases} \quad (8)$$

$$\{\!\!\{ v \}\!\!\} := \begin{cases} \frac{1}{2}(v|_K + v|_{K'}) & \text{on } \gamma = \partial K \cap \partial K' \\ v|_K & \text{on } \gamma = \partial K \cap \Gamma_D \end{cases} \quad \{\!\!\{ \vec{v} \}\!\!\} := \begin{cases} \frac{1}{2}(\vec{v}|_K + \vec{v}|_{K'}) & \text{on } \gamma = \partial K \cap \partial K' \\ \vec{v}|_K & \text{on } \gamma = \partial K \cap \Gamma_D \end{cases} \quad (9)$$

Here $v|_K$ denotes the trace of v onto the edge $\gamma \in \mathcal{E}(K) \cap \mathcal{E}(K')$ and \vec{n}_K is the outward unit vector relative to K on γ . For $\gamma \subset \Gamma$, we define $\{\!\!\{ v \}\!\!\} := v$, $\{\!\!\{ \vec{v} \}\!\!\} := \vec{v}$, $[\![v]\!] := v\vec{n}_\Omega$, and $[\![\vec{v}]\!] := \vec{v} \cdot \vec{n}_\Omega$.

To account for the singular behaviour of solutions near singular points of the polygon Ω , we define the set

$$\mathcal{K}_0 = \{K \in \mathcal{T} : P \in \overline{K} \text{ for some } P \in SP(\Omega, \Gamma_D, \Gamma_N)\}. \quad (10)$$

Let $K \in \mathcal{K}_0$. We will assume the mesh is graded enough such that exactly one singular point belongs to \overline{K} . The corresponding vertex is denoted by A_K and the corresponding weight β_K . Moreover, the spaces $H_{\beta_k}^{m,l}(K)$ are equipped with the weight function $\Phi_{\beta_K}(\vec{x}) = r_K^{\beta_K}$, where $r_K = |\vec{x} - A_K|$. We conclude the section by stating the following lemmas [Wih03]:

Lemma 4 (Trace inequalities [Wih03, Lemma A.2.4]) *Let $\gamma \in \mathcal{E}(K)$. Then, there holds*

1. if $u \in H^2(K)$ and $u = 0$ at the vertices of K , then the trace $u|_\gamma \in H^1(\gamma)$ and

$$\begin{aligned} \|u\|_{H^1(\gamma)}^2 &\leq Ch_K |u|_{H^2(K)}^2 \\ \|u\|_{L^2(\gamma)}^2 &\leq Ch_K^3 |u|_{H^2(K)}^2. \end{aligned} \quad (11)$$

2. if $u \in H_{\vec{\beta}}^{2,2}(\Omega)$, $0 < \beta < 1$, and $u = 0$ at the vertices of K , then

$$\begin{aligned} \|u\|_{H^1(\gamma)}^2 &\leq Ch_K^{1-2\beta} |u|_{H_{\vec{\beta}}^{2,2}(K)}^2 \\ \|u\|_{L^2(\gamma)}^2 &\leq Ch_K^{3-2\beta} |u|_{H_{\vec{\beta}}^{2,2}(K)}^2, \end{aligned} \quad (12)$$

if γ does not contain any vertex A_i , $i = 1, \dots, M$.

Lemma 5 (Continuity at the interior edges [Wih03, Lemma 1.3.4]) *Let $u \in H_{\vec{\beta}}^{1,1}(\Omega)$ for $0 \leq \vec{\beta} \leq 1$. Then, for an interior edge $\gamma \in \mathcal{E}_I$ there holds $[\![u]\!] = 0$ a.e. on γ .*

2.3 Variational formulation of the Poisson equation

Here, we define the SIP-dG variational formulation of problem (4) and state its consistency.

Definition 2.1 (SIP-dG of the Poisson equation) *Define the bilinear form \mathcal{A}_h by*

$$\begin{aligned} \mathcal{A}_h(u, v) := & \sum_{K \in \mathcal{T}} \int_K \nabla_h u \cdot \nabla_h v \, d\vec{x} \\ & - \sum_{\gamma \in \mathcal{E}_I \cup \mathcal{E}_D} \int_\gamma ([\![v]\!] \cdot \{\!\!\{ \nabla_h u \}\!\!\} + [\![u]\!] \cdot \{\!\!\{ \nabla_h v \}\!\!\}) \, ds \\ & + \sum_{\gamma \in \mathcal{E}_I \cup \mathcal{E}_D} \int_\gamma \sigma [\![u]\!] \cdot [\![v]\!] \, ds, \end{aligned} \quad (13)$$

and the corresponding linear functional l_h by

$$l_h(v) := \sum_{K \in \mathcal{T}} \int_K f v \, d\vec{x} + \int_{\Gamma_N} g v \, ds - \sum_{\gamma \in \mathcal{E}_D} \int_{\gamma} (\nabla_h v \cdot \vec{n}_{\Omega}) u_D \, ds + \sum_{\gamma \in \mathcal{E}_D} \frac{\sigma}{|\gamma|} \int_{\gamma} u_D v \, ds, \quad (14)$$

where $\sigma > 0$ is the, so called, discontinuity penalisation parameter, given by

$$\sigma := C_{\sigma} \frac{p^2}{h}. \quad (15)$$

The constant $C_{\sigma} > 0$ is typically chosen large enough so as to achieve coercivity.

Then, the SIP-dG method of the Poisson problem (4) reads as: Find $u_h \in \mathbb{V}$ such that

$$\mathcal{A}_h(u_h, v_h) = l_h(v_h) \quad \forall v_h \in \mathbb{V}. \quad (16)$$

Some basic properties of the SIP-dG method, such as existence and uniqueness of the result, have been proved in [Wih03]. In particular, we are interested in the subsequent analysis to the following proposition:

Proposition 6 (Consistency of the SIP-dG method) *For $f \in H_{\vec{\beta}}^{0,0}(\Omega)$, $u_D \in H_{\vec{\beta}}^{3/2,3/2}(\Gamma_D)$, $g \in H_{\vec{\beta}}^{1/2,1/2}(\Gamma_N)$, the bilinear form and the linear functional in Definition 2.1 are well-defined and the SIP-dG method is consistent:*

$$\mathcal{A}_h(u, v_h) - l_h(v_h) = 0 \quad \forall v_h \in \mathbb{V}, \quad (17)$$

where $u \in H_{\vec{\beta}}^{2,2}(\Omega)$ is the exact solution of (4). Let $e = u - u_h$ be the error in the SIP-dG method. Using the previous result the following Galerkin orthogonality holds:

$$\mathcal{A}_h(e, v_h) = 0 \quad \forall v_h \in \mathbb{V}. \quad (18)$$

3 A-posteriori error estimate of the SIP-dG method

We consider the dual problem of (4):

$$\begin{aligned} -\Delta\phi &= e \text{ in } \Omega \\ \phi &= 0 \text{ on } \Gamma. \end{aligned} \quad (19)$$

Since $e \in \mathbb{V} \subset H_{\vec{\beta}}^{0,0}(\Omega)$, the conditions of Theorem 2 are satisfied and the problem (19) admits a (weak) solution $\phi \in H_{\vec{\beta}}^{2,2}(\Omega)$. Moreover

$$\mathcal{A}_h(\phi, v_h) = l_h(v_h) = \langle e, v \rangle_{L^2(\Omega)} \quad \forall v_h \in \mathbb{V}, \quad (20)$$

where $\langle \cdot, \cdot \rangle_{L^2(\Omega)}$ on right hand side (rhs) denotes the standard inner product in $L^2(\Omega)$. This can be used for the derivation of general goal oriented estimators, which can affect the properties of the resulting adapted mesh. We now state the following proposition and lemmas, that will be used for the derivation of the L^2 a-posteriori error estimator:

Proposition 7 (Regularity of the solution on weighted Sobolev Spaces) *Due to Theorem 2.1 [BG88], if $e \in H_{\vec{\beta}}^{k,0}(\Omega)$, for $k \geq 0$, there exists $\phi \in H_{\vec{\beta}}^{k+2,2}(\Omega)$, where $\vec{\beta}$ depends on the opening angles at the vertices of Ω , such that*

$$\|\phi\|_{H_{\vec{\beta}}^{k+2,2}(\Omega)} \leq C(k) \|e\|_{H_{\vec{\beta}}^{k,0}(\Omega)}. \quad (21)$$

Since $e \in \mathbb{V} \subset H_{\vec{\beta}}^{2,2}(\Omega)$, we can take $k = 0$ and exploit Remark (1) to obtain

$$\|\phi\|_{H_{\vec{\beta}}^{2,2}(\Omega)} \leq C \|e\|_{L^2(\Omega)}. \quad (22)$$

Lemma 8 (Nodal interpolants for dG-FEM) *For an element $K \in \mathcal{T}/\mathcal{K}_0$, let $\Pi_K : \mathcal{C}^0(\bar{K}) \rightarrow \mathcal{P}^1(K)$ denote the piece-wise linear operator into polynomials of degree at most one. By standard interpolation results [BS08] there holds*

$$\|v - \Pi_K v\|_{L^2(K)} \leq Ch_K \|v\|_{H^1(K)}. \quad (23)$$

In corner elements $K \in \mathcal{K}_0$, the interpolation bounds in [Wih03; Sch98] (Lemma 2.5.3.) for the linear interpolant in the weighted space $H_{\vec{\beta}}^{2,2}(K)$ for $\beta_K \in [0, 1)$ gives

$$\|v - \Pi_K v\|_{H^1(K)} \leq Ch_K^{1-\beta_K} \|v\|_{H_{\beta_K}^{2,2}(K)}. \quad (24)$$

Lemma 9 (Discrete trace inequality [EG21]) *Assuming that $P \subset L^\infty(K)$, there exists a constant c such that the following holds:*

$$\|v\|_{L^p(F, \mathbb{R}^n)} \leq c h_K^{-\frac{1}{p} + n(\frac{1}{p} - \frac{1}{r})} \|v\|_{L^r(K, \mathbb{R}^n)}, \quad (25)$$

for all $p, r \in [1, \infty]$, all $v \in P_K$, all $K \in \mathcal{T}$, and all the faces F of K .

We can now proceed with the derivation of the estimator. We start by taking $v_h = e$ in equation (20) and exploit the Galerkin orthogonality for the linear interpolant $\Pi_h v$, defined as $\Pi_h v|_K = \Pi_K v$. We have that $\Pi_K v \subset \mathcal{C}^0(K) \subset \mathbb{V}$. Then, using the Galerkin orthogonality (18)

$$\begin{aligned} \|e\|_{L^2(\Omega)}^2 &= \mathcal{A}_h(\phi, e) = \mathcal{A}_h(\phi - \Pi_h \phi, e) = \sum_{K \in \mathcal{T}} \int_K \nabla_h(\phi - \Pi_h \phi) \cdot \nabla_h e \, d\vec{x} \\ &\quad - \sum_{\gamma \in \mathcal{E}_I} \int_\gamma (\llbracket \phi - \Pi_h \phi \rrbracket \cdot \llbracket \nabla_h e \rrbracket + \llbracket e \rrbracket \cdot \llbracket \nabla_h(\phi - \Pi_h \phi) \rrbracket) \, ds. \end{aligned} \quad (26)$$

Integration by parts of the first term on the rhs gives

$$\begin{aligned} \|e\|_{L^2(\Omega)}^2 &= \sum_{K \in \mathcal{T}} \int_K (\phi - \Pi_h \phi)(f + \Delta_h u_h) \, d\vec{x} \\ &\quad + \sum_{\gamma \in \mathcal{E}_I} \int_\gamma \left((\phi - \Pi_h \phi) \llbracket \nabla_h u_h \rrbracket + \llbracket u_h \rrbracket \cdot \llbracket \nabla_h(\phi - \Pi_h \phi) \rrbracket \right) \, ds, \end{aligned}$$

where we have also exploited Remark 1 and Lemma 5 on u and $\nabla_h u$, respectively. We then apply the Cauchy-Schwartz inequality:

$$\begin{aligned} \|e\|_{L^2(\Omega)}^2 &\leq \sum_{K \in \mathcal{K}_0} \|\phi - \Pi_h \phi\|_{L^2(K)} \|f + \Delta_h u_h\|_{L^2(K)} + \sum_{K \in \mathcal{T}/\mathcal{K}_0} \|\phi - \Pi_h \phi\|_{L^2(K)} \|f + \Delta_h u_h\|_{L^2(K)} \\ &+ \sum_{\gamma \in \mathcal{E}_I} \|\phi - \Pi_h \phi\|_{L^2(\gamma)} \|\llbracket \nabla_h u_h \rrbracket\|_{L^2(\gamma)} + \sum_{\gamma \in \mathcal{E}_I} \|\llbracket u_h \rrbracket\|_{L^2(\gamma)} \|\nabla_h \{\phi - \Pi_h \phi\}\|_{L^2(\gamma)}. \end{aligned} \quad (27)$$

For the first term we have by Lemma 8 and Proposition 7 that

$$\|\phi - \Pi_h \phi\|_{L^2(K)} \leq Ch_K \|\phi - \Pi_h \phi\|_{H^1(K)} \leq Ch_K^{2-\beta_K} |\phi|_{H_{\beta_K}^{2,2}(\Omega)} \leq Ch_K^{2-\beta_K} \|e\|_{L^2(\Omega)} \quad \forall K \in \mathcal{K}_0. \quad (28)$$

For the second term, Lemma 8 gives

$$\|\phi - \Pi_h \phi\|_{L^2(K)} \leq Ch_K^2 |\phi|_{H^2(K)} \leq Ch_K^2 \|e\|_{L^2(\Omega)} \quad \forall K \in \mathcal{T}/\mathcal{K}_0. \quad (29)$$

For the remaining two terms we have:

$$\begin{aligned} \|\phi - \Pi_K \phi\|_{L^2(\gamma)} &\leq C\sqrt{h_K} \|\phi - \Pi_K \phi\|_{H^1(K)} \\ &\leq \begin{cases} Ch_K^{3/2-\beta_K} \|\phi\|_{H_{\beta_K}^{2,2}(K)} \leq Ch_K^{3/2-\beta_K} \|e\|_{L^2(\Omega)} & \text{if } \gamma \in K \in \mathcal{K}_0, \\ Ch_K^{3/2} \|\phi\|_{H^2(K)} \leq Ch_K^{3/2} \|e\|_{L^2(\Omega)} & \text{if } \gamma \in K \notin \mathcal{K}_0. \end{cases} \end{aligned} \quad (30)$$

Using Lemma 9 we obtain the upper bound:

$$\begin{aligned} \|\{\nabla_h(\phi - \Pi_K \phi)\}\|_{L^2(\gamma)} &\leq Ch_K^{-1/2} \|\nabla_h(\phi - \Pi_K \phi)\|_{L^2(K)} \\ &\leq h_k^{-1/2} \|\phi - \Pi_K \phi\|_{H^1(K)} \\ &\leq \begin{cases} Ch_k^{1/2-\beta_K} \|e\|_{L^2(\Omega)} & \text{if } \gamma \in K \in \mathcal{K}_0, \\ Ch_k^{1/2} \|e\|_{L^2(\Omega)} & \text{if } \gamma \in K \notin \mathcal{K}_0. \end{cases} \end{aligned} \quad (31)$$

Replacing the results obtained in (28)-(31) in equation (27) we have:

$$\begin{aligned} \|e\|_{L^2(\Omega)} &\leq C_1 \sum_{K \in \mathcal{K}_0} \left(h_K^{2-\beta_K} \|f + \Delta_h u_h\|_{L^2(K)} + \right. \\ &\quad \left. \frac{1}{2} \sum_{\partial K \in \mathcal{E}(K)} (h_K^{3/2-\beta_K} \|\nabla_h u_h\|_{L^2(\partial K)} + h_K^{1/2-\beta_K} \|u_h\|_{L^2(\partial K)}) \right) \\ &+ C_2 \sum_{K \in \mathcal{T}/\mathcal{K}_0} \left(h_K^2 \|f + \Delta_h u_h\|_{L^2(K)} + \frac{1}{2} \sum_{\partial K \in \mathcal{E}(K)} (h_K^{3/2} \|\nabla_h u_h\|_{L^2(\partial K)} + h_K^{1/2} \|u_h\|_{L^2(\partial K)}) \right). \end{aligned} \quad (32)$$

This expression can be simplified if $u \in \mathbb{V}$ with $p = 1$ and $f = 0$. We further introduce the indicator function $\mathbb{1}_{\gamma \in \mathcal{E}_I(\mathcal{K}_0)}$ and rewrite (32) in the more compact form

$$\begin{aligned} \|e\|_{L^2(\Omega)} &\leq \sum_{\gamma \in \mathcal{E}_I} (h_{K(\gamma)}^{3/2-\mathbb{1}_{\gamma \in \mathcal{E}_I(\mathcal{K}_0)}\beta_\gamma} \|\llbracket \nabla_h u_h \rrbracket\|_{L^2(\gamma)} + h_{K(\gamma)}^{1/2-\mathbb{1}_{\gamma \in \mathcal{E}_I(\mathcal{K}_0)}\beta_\gamma} \|\llbracket u_h \rrbracket\|_{L^2(\gamma)}) \\ &\leq \left(\sum_{\gamma \in \mathcal{E}_I} h_{K(\gamma)}^{3-1_{\gamma \in \mathcal{E}_I(\mathcal{K}_0)}2\beta_\gamma} \|\llbracket \nabla_h u_h \rrbracket\|_{L^2(\gamma)}^2 + h_{K(\gamma)}^{1-1_{\gamma \in \mathcal{E}_I(\mathcal{K}_0)}2\beta_\gamma} \|\llbracket u_h \rrbracket\|_{L^2(\gamma)}^2 \right)^{1/2}. \end{aligned} \quad (33)$$

For practical purposes, we reformulate (33) for each K in order to obtain a cell-wise error indicator:

$$\|e\|_{L^2(\Omega)}^2 \leq \sum_{K \in \mathcal{T}} \sum_{\gamma \in \mathcal{E}_I(K)} h_K^{3-1_{\gamma \in \mathcal{E}_I(\mathcal{K}_0)}2\hat{\beta}_\gamma} \|\llbracket \nabla_h u_h \rrbracket\|_{L^2(\gamma)}^2 + h_K^{1-1_{\gamma \in \mathcal{E}_I(\mathcal{K}_0)}2\hat{\beta}_\gamma} \|\llbracket u_h \rrbracket\|_{L^2(\gamma)}^2, \quad (34)$$

where $\hat{\beta} \in [0, 1]$ replaces the weight β , whose range is specified in Remark 3. Here, actually, $\hat{\beta}$ defines an upper bound for the L^2 error and does not prevent the solution u of problem 4 to lie in an admissible weighted Sobolev space.

4 Numerical Results

In this section we consider as model problem the Poisson equation

$$\begin{aligned} -\Delta u &= 0 \text{ in } \Omega \\ u_D(r, \theta) &= r^{\pi/\omega} \sin(\pi\theta/\omega) \text{ on } \Gamma, \end{aligned} \quad (35)$$

where $\omega \in (\pi, 2\pi)$ is the angle of the re-entrant corner located at $\vec{0} = (0, 0) \in \mathbb{R}^2$. We evidence that u is analytic in $\bar{\Omega}/\{\vec{0}\}$ and $u \notin H^2(\Omega)$, so that $SP(\Omega, \Gamma_D, \Gamma_N) = \{A_1 := \vec{0}\}$. Therefore, the weight function is defined as $\Phi_\beta(\vec{x}) = |\vec{x}|^\beta$, where $\beta \in (1 - \frac{\pi}{\omega}, 1]$, according to Remark 3. Let Ω be the L-shaped domain $(-1, 1)^2/[0, 1] \times (-1, 0]$. Then, the harmonic solution of problem (35) is

$$u(r, \theta) = r^{2/3} \sin(2\theta/3). \quad (36)$$

We compare the accuracy of the SIP-dG method applied to problem (35) using different adaptive mesh strategies and assess the quality of the resulting meshes in §4.3. For all the tests, we compute the numerical solution $u_h \in \mathbb{V}$ with $p = 1$. All the tests have been performed in FEniCS [LW10].

4.1 h-refinement

In the h -adaptive process, we introduce the global error indicator $\eta^2 = \sum_{K \in \mathcal{T}} \eta_K^2$, where η_K^2 refers to each cell K on the rhs of equation (34). As a widely accepted criterion, elements with large error estimator should be marked for refinement. Here, we employ the so called *maximum strategy (ms)*, which can be described as follows

$$\eta_K \geq \alpha \max_{K' \in \mathcal{T}} \eta_{K'} \iff K \text{ is marked for refinement}, \quad (37)$$

where $\alpha \in (0, 1)$ is a predetermined parameter. The steps involved in the ms h -refinement are given below:

1. Compute the error indicators $\{\eta_K \mid K \in \mathcal{T}\}$ for each cell according to equation (34).
2. Mark elements for refinement using equation (37).

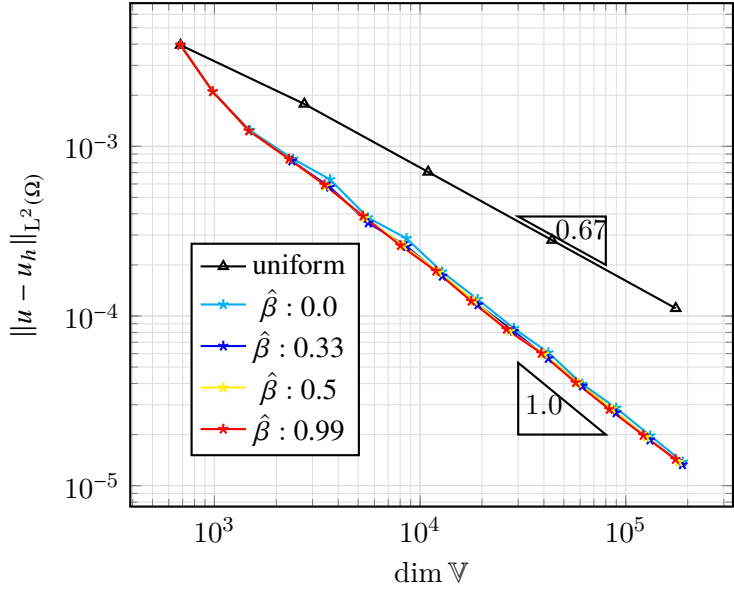
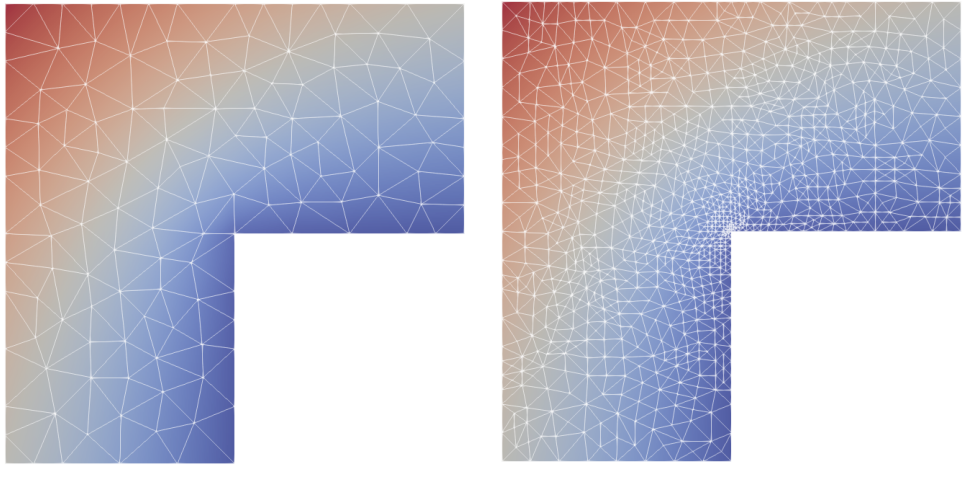


Figure 1: Asymptotic convergence rates for the h-refinement strategy on the finite element space \mathbb{V} . Note that the rate of convergence is optimal and independent on $\hat{\beta}$. Uniform mesh refinement yields a convergence rate of $2/3$ due to the singular behaviour of the solution near the origin [GMP17].



(a) Initial unstructured mesh.

(b) mesh refined after 4 iterations.

Figure 2: Solution of eq.(35) with h -refinement ($\hat{\beta} = 0.0$).

3. Refine each marked element by edge bisection.

The *ms* h -refinement strategy with $\alpha = 0.1$ has been tested for different $\hat{\beta}$. As visible in Fig.3, the level of refinement is increasing near the corner as a function of $\hat{\beta}$. It appears from Fig.1 that $\hat{\beta} = 0.0$ is already sufficient for achieving an optimal order of convergence.

4.2 r-adaptive strategy

The r-adaptive strategy aims to generate an adapted mesh \mathcal{T} by relocating a fixed number of mesh points. This process can be interpreted as the image from a computational domain Ω_c , having a fixed mesh \mathcal{T}_c ,

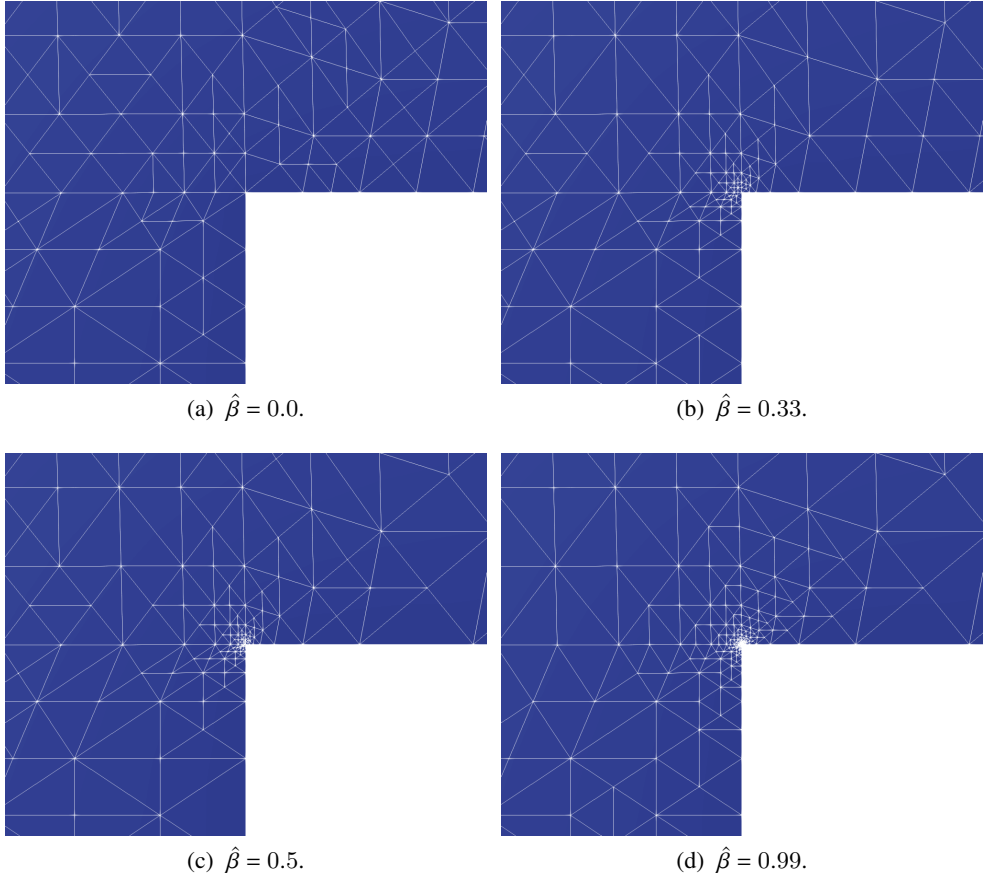


Figure 3: Solution of eq.(35) near the origin after 14 h-refinements.

to a physical domain Ω , with variable mesh \mathcal{T}_i . The first method we propose is a variational one, where the transformation mapping is determined as the minimiser of an adaptation functional [BHR09; Win66]. The Moving Mesh PDE (MMPDE) associated with the minimiser will be solved by the Euler-Lagrange equation.

An adaptive mesh based on *Optimal Transport* will be also constructed in the last Subsection [BHR09]. This method exploits the strong dependence of the solution on the radial variable, which yields a mesh with high shape regularity and optimal convergence rate. A major advantage of the OT strategy is the computational efficiency, as the adapted mesh is obtained after solving a one dimensional algebraic equation for each node. On the contrary, the implementation of the other r-adaptive methods requires a more computationally expensive iterative procedure.

4.2.1 Winslow's diffusion method

The Winslow' diffusion method is defined by the smooth mapping $\vec{x} = (x, y) = \vec{x}(\vec{\xi}) : \Omega_c \rightarrow \Omega$ or the inverse coordinate transformation $\vec{\xi} = (\xi, \eta) = \vec{\xi}(\vec{x}) : \Omega \rightarrow \Omega_c$. Practically, most of the MMPDEs were developed in terms of the inverse coordinate transformation, as this guarantees existence and uniqueness of the solution [Win66; Dvi91]. Thus, we will first solve the MMPDE associated with $\vec{\xi}(\vec{x})$ and the determine the transformed coordinate $\vec{x}(\vec{\xi})$ by change of variable. Consider the functional

$$I_{Win}[\vec{\xi}] = \frac{1}{2} \int_{\Omega} \frac{1}{w(\vec{x})} \sum_i (\nabla \xi_i)^T (\nabla \xi_i) d\vec{x}, \quad (38)$$

where $w(\vec{x}) > 0$ is a given monitor function. This function can be chosen to depend on the solution $u_h(\vec{x})$ of the physical PDE. We consider as possible choices:

1. Gradient:

$$w|_K = \left(1 + \frac{1}{\delta} |\nabla_h u_h|^2 \right)^{1/2} \quad (39)$$

2. Curvature:

$$w|_K = \left(1 + \frac{1}{\delta} |\Delta_h u_h| \right)^{1/2} \quad (40)$$

3. A-posteriori:

$$w|_K = \left(1 + \frac{1}{\delta} \eta_K^2 \right)^{1/2} \quad (41)$$

where δ is a prescribed intensity parameter for \mathcal{T} [HR11; BHR09]. The MMPDE associated with the functional (38) becomes

$$\partial_s \vec{x}(\vec{\xi}, s) = - \sum_{i=1} \vec{a}_i \nabla \cdot (\vec{M}^{-1} \vec{a}^i), \quad (42)$$

where s denotes the temporal variable, $\vec{a}^i = \nabla \xi_i$, $\vec{a}_i = \partial \vec{x} / \partial \xi_i$, and $\vec{M} = w(\vec{x}) I_2$ is the metric function. The replacement of the previous terms in the two-dimensional space gives

$$\begin{aligned} \partial_s \vec{x}(\vec{\xi}, s) = \frac{1}{J^2 w^2} & \left[(x_\eta^2 + y_\eta^2) \frac{\partial}{\partial \xi} \left(w \frac{\partial \vec{x}}{\partial \xi} \right) - (x_\xi x_\eta + y_\xi y_\eta) \frac{\partial}{\partial \eta} \left(w \frac{\partial \vec{x}}{\partial \xi} \right) \right. \\ & \left. - (x_\xi x_\eta + y_\xi y_\eta) \frac{\partial}{\partial \xi} \left(w \frac{\partial \vec{x}}{\partial \eta} \right) + (x_\xi^2 + y_\xi^2) \frac{\partial}{\partial \eta} \left(w \frac{\partial \vec{x}}{\partial \eta} \right) \right]. \end{aligned} \quad (43)$$

This PDE allows us to compute $\vec{x}(\vec{\xi}, s_{i+1})$ and hence \mathcal{T}_{i+1} given the knowledge of $w(\vec{x})$ and \mathcal{T}_c . Equation (43) is discretised in space using the FEM with linear Lagrangian elements and in time with the semi-implicit Euler method. To that purpose, we divide the temporal domain $[0, S]$ into a partition of N_S consecutive subintervals $0 = s_0 < s_1 < \dots < s_{N_S} = S$ with $s_i - s_{i-1} = k$ for all i . We treat the non-linear terms through evaluation at the current time step s_i , while the linear terms are evaluated at the next time step s_{i+1} . For further implementation details we refer the reader to Chapter ??-§??.

Dirichlet boundary condition are imposed on all the edges except for that ones intersecting at the re-entrant corner. For those, the monitor function $w(\vec{\xi})$ has been first projected onto the two sides and the solution of the MMPDE5 [HR11] in one dimension is computed. This results in the movement of the mesh points towards the origin.

The non-convex domain Ω poses a practical complication for the application of Winslow's MMPDE. In fact, it is well known that if the computational domain Ω_c is not convex, the resulting physical mesh might feature very skewed or even overlapping elements. A natural solution for that issue is to define a computational mesh that is convex and solve for the coordinate transformation $\vec{x}(\vec{\xi})$ on this domain [WWR99; LTZ01]. Once Ω_c is selected, a mesh \mathcal{T}_c with the same topology as \mathcal{T} can be constructed by first specifying a correspondence between the boundaries $\partial\Omega$ and $\partial\Omega_c$ by a mapping $g(\vec{x})$ and then let \mathcal{T}_c be the image of \mathcal{T} under the mapping $\vec{\xi}(\vec{x})$ satisfying

$$\begin{aligned} \Delta \vec{\xi}(\vec{x}) &= 0 \text{ in } \Omega \\ \vec{\xi} &= g(\vec{x}) \text{ on } \partial\Omega. \end{aligned} \tag{44}$$

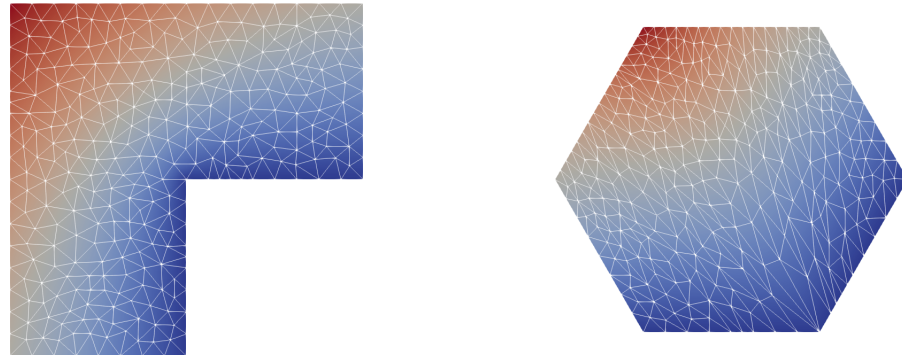


Figure 4: Solution of eq.(35) represented in the physical and computational domain.



Figure 5: x and y coordinates represented in the computational mesh \mathcal{T}_c , obtained as solution of eq.(44). The boundary conditions match with that ones of the physical domain.

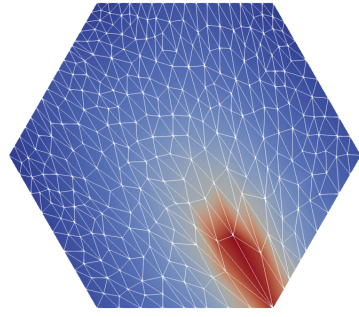
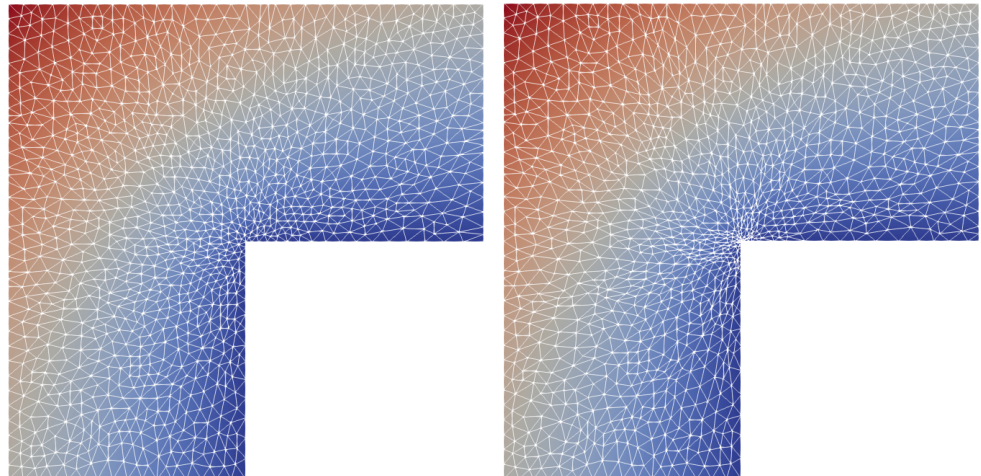
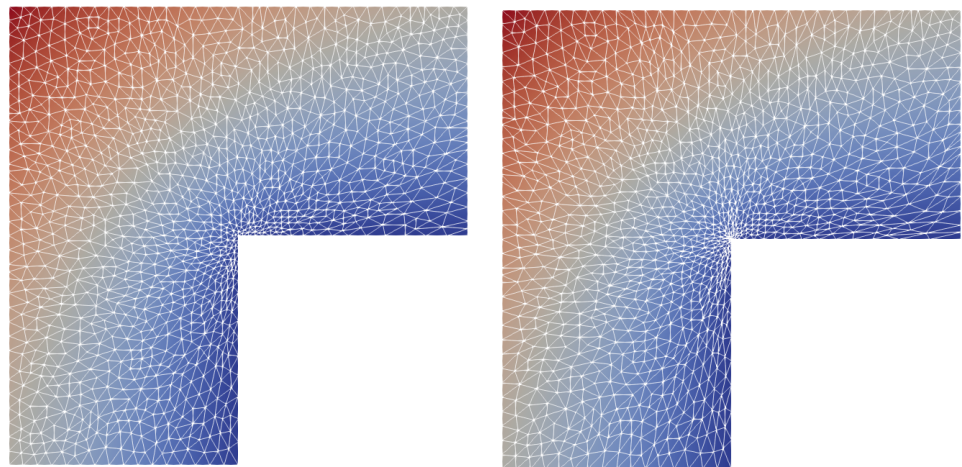


Figure 6: Monitor function $w(\vec{\xi})$ in the computational domain.



(a) Mesh adapted with gradient monitor function. (b) Mesh adapted with curvature monitor function.



(c) Mesh adapted with a-posteriori monitor function
($\hat{\beta} = 0.0$). (d) Mesh adapted with a-posteriori monitor function
($\hat{\beta} = 0.99$).

Figure 7: Solution of eq.(35) with Winslow's MMPDE for different monitor functions with $\dim \mathbb{V} = 7005$.

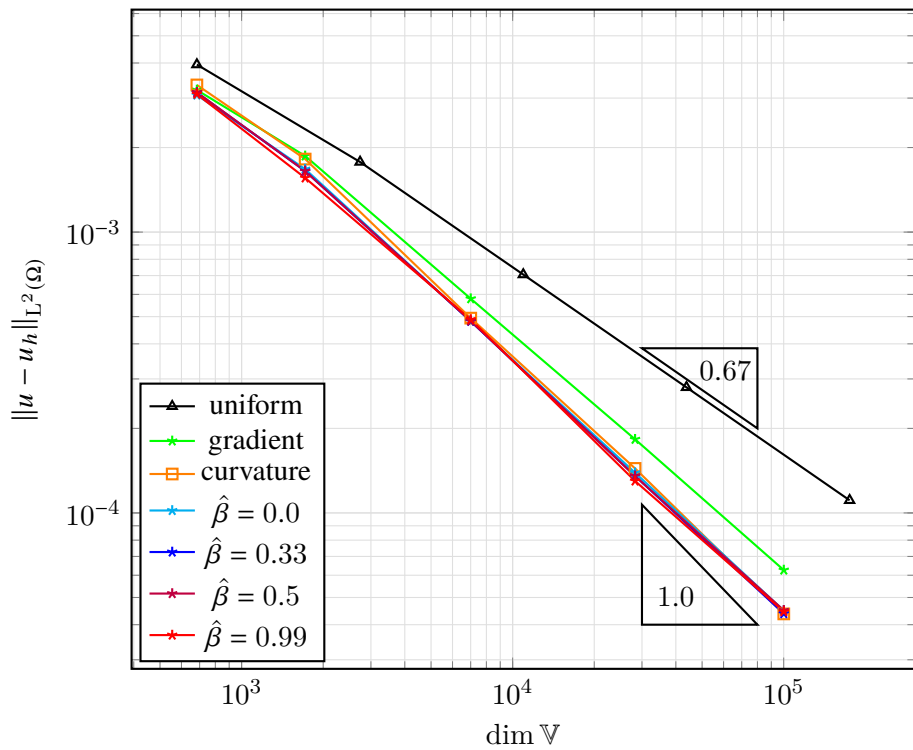
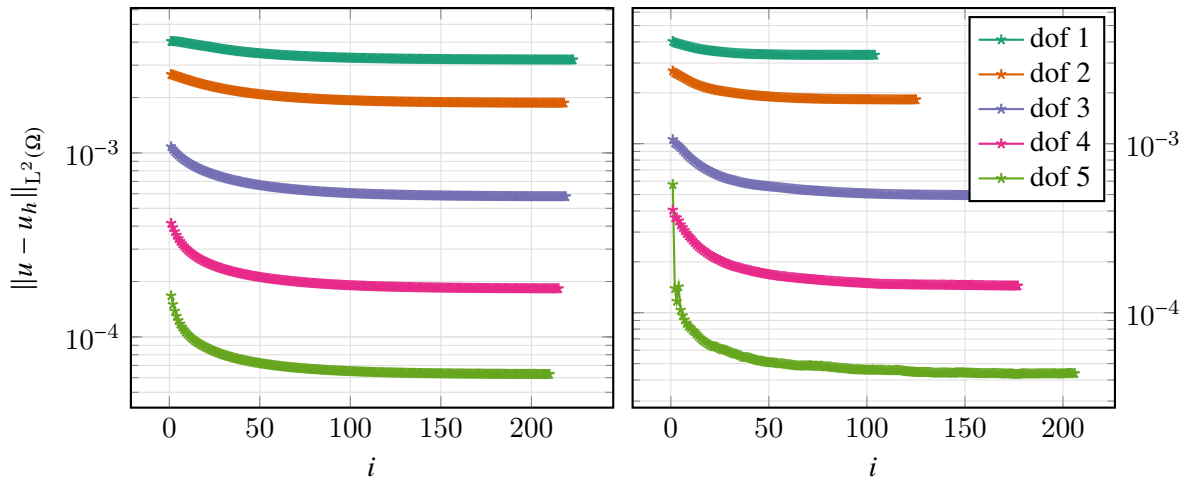
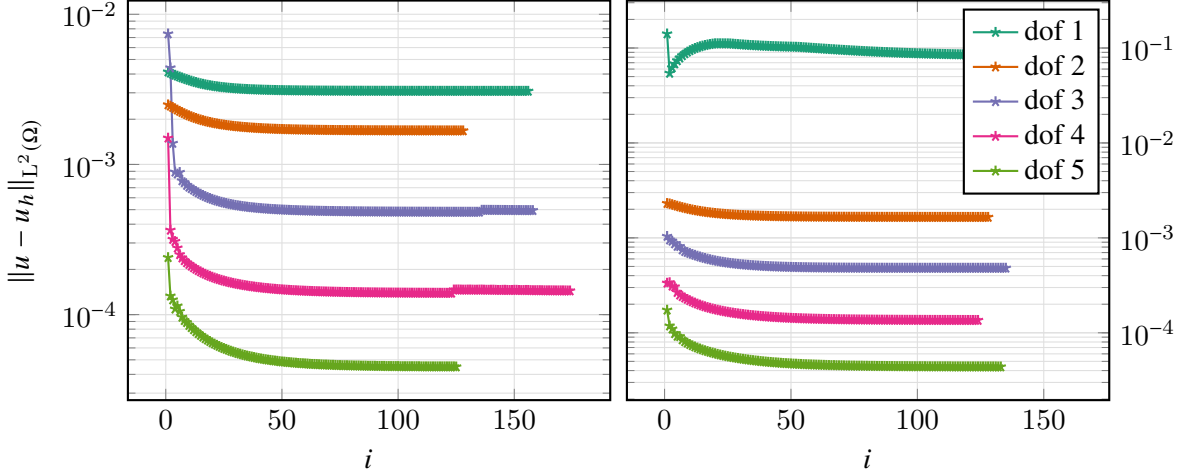


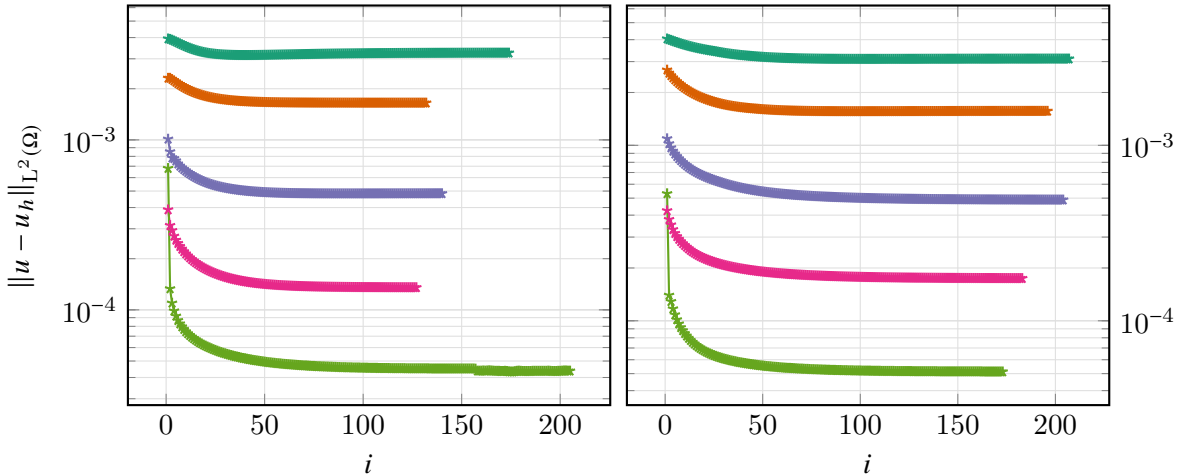
Figure 8: Asymptotic convergence rates of Winslow's MMPDE for different monitor functions w (39)-(41).



(a) Solution error as a function of iterations of the MMPDE with gradient monitor function.
(b) Solution error as a function of iterations of the MMPDE with curvature monitor function.



(a) Solution error as a function of iterations of the MMPDE with a-posteriori monitor function ($\hat{\beta} = 0.0$). (b) Solution error as a function of iterations of the MMPDE with a-posteriori monitor function ($\hat{\beta} = 0.33$).



(c) Solution error as a function of iterations of the MMPDE with a-posteriori monitor function ($\hat{\beta} = 0.5$). (d) Solution error as a function of iterations of the MMPDE with a-posteriori monitor function ($\hat{\beta} = 0.99$).

Figure 9: The solution error decreases monotonically over the iterations until reaching convergence for all the monitor functions. The relative tolerance has been fixed to 1×10^{-5} , while the timestep has been set to $k = 10^{-3}$. The degrees of freedom (dof) appearing in the legend are 684, 1716, 7005, 28290, and 100080.

4.2.2 Optimal Transport mesh

We devise a mesh for the L-shaped region by solving the Monge-Ampère equation close to the re-entrant corner. The solution is then tuned to match the boundary of the domain.

Local mesh scaling We start by assuming that the interpolation error of $u_h(r)$ is strongly dependent on r and weakly dependent on θ , so that $u_h(r) \sim h^2 \frac{d^2}{dr^2} u$, where h is the local mesh size of an element close to the corner and r is the distance from the origin. The error is dominated by $E_{max} = h^2 r^{2/3-2}$. Following the *equidistribution principle*, we seek to equidistribute E_{max} , so that we obtain $h \sim r^{2/3}$. Given the computation variable s , which represents the distance from the origin in the computational domain $\Omega_c \equiv \Omega$, we can interpret h as being proportional to dr/ds . Solving the differential equation $\frac{dr}{ds} = h = r^{2/3}$ we obtain that $r \sim s^3$.

Solution of Monge-Ampère equation We now look for a radially symmetric transformation from the corner region to itself. More details and extensions of this application can be found in [BRW15]. Locally, the first integral of the Monge-Ampère equation implies that r satisfies the Ordinary Differential Equation (ODE) in polar coordinates:

$$m(r) r dr d\theta = s ds d\theta, \quad (45)$$

where $m(r) = r^\gamma$ is the monitor function, which will be determined by the *a-priori* estimate for the interpolation error:

$$r^\gamma r r^{2/3} = r^{1/3},$$

so that $\gamma = -4/3$.

We expect that for large r the adapted mesh is almost regular, so that $m(r) \sim 1$ far from the corner, and consider the general expression

$$m(r) = \alpha + \beta r^{-4/3}, \quad \alpha, \beta \in \mathbb{R}, \quad (46)$$

where α and β are two regularisation parameters.

From (45) we integrate over the variable θ and obtain

$$\left(\alpha + \beta r^{-4/3} \right) r \frac{dr}{ds} = s,$$

so that r satisfies the nonlinear algebraic equation

$$\alpha r^2 + 3\beta r^{2/3} = s^2. \quad (47)$$

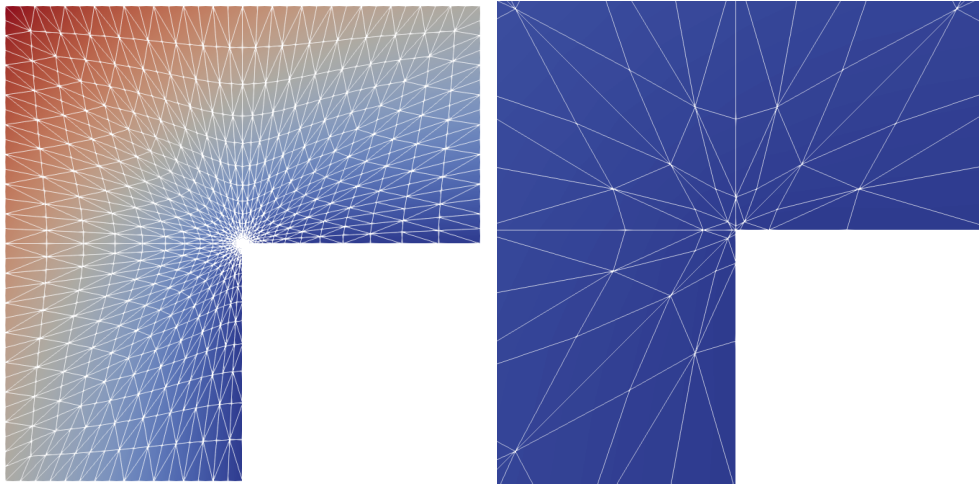
The equation (47) then determines the mesh transformation. Note that the parameter α and β controls the level of mesh compression near the corner. In fact, for high values of β we have $r \sim s^3$, whereas for large α we have $r \sim s$. For the remainder of the analysis, we choose $\beta = 1/3$, as this is the maximum admissible value that satisfies the boundary condition $\alpha + 3\beta = 1$ in equation (47), when $r, s = 1$.

Computation of the OT mesh Suppose we have a uniform regular mesh $(\xi_{i,j}, \eta_{i,j})$ in Ω_c that we want to map to an adapted non-uniform mesh $(x_{i,j}, y_{i,j})$ in the physical domain, with $i, j = 1, \dots, N$. The application of the Monge-Ampère method provides the desired mesh as follows:

1. For each pair (i, j) , compute $s_{i,j}^2 = \xi_{i,j}^2 + \eta_{i,j}^2$.
2. Compute the angle $\theta_{i,j}$ with respect to the semi-positive x axis by $\arctan\left(\frac{\eta_{i,j}}{\xi_{i,j}}\right)$.

3. Compute the length $l_{i,j}$ of the straight line spanned from the origin with angle $\theta_{i,j}$ to the boundary of the L-shaped domain.
4. Set $\beta = 1/3$ and enforce the condition $m = \alpha + \beta l_{i,j}^{-4/3} = 1$, which leads to $\alpha = 1 - 3\beta l_{i,j}^{-4/3}$. This ensures that the new mesh boundaries match the L-shaped ones.
5. Solve equation (47) to find $r_{i,j}$.
6. Set $(x_{i,j}, y_{i,j}) = \frac{r_{i,j}}{s_{i,j}}(\xi_{i,j}, \eta_{i,j})$.

Given the new mesh $(x_{i,j}, y_{i,j})$, we can increase the dofs by uniform refinement or by applying the previous procedure from a more graded uniform mesh. The first approach is less computationally expensive and provides higher accuracy.



(a) Mesh adapted with the Monge-Ampère equation. (b) Zoom of the solution in the re-entrant corner.

Figure 10: Solution of eq.(35) on the OT mesh.

4.3 Quality of the mesh

The errors in the solution of equation (35) are critically dependent on the nature on the resulting mesh. The quality of a mesh can be expressed in terms of *shape regularity* or, in the context of SIP-dG method, by the *mesh condition*:

$$\|\llbracket h \rrbracket / \{ h \}\|_{L^\infty_{\mathcal{E}_I}}, \quad (48)$$

with h denoting the element-wise constant function characterising the local meshsize. The condition $\|\llbracket h \rrbracket / \{ h \}\|_{L^\infty_{\mathcal{E}_I}} \leq \alpha$, for some $0 \leq \alpha < 1$ small enough, has been used to prove the inf-sup stability of the SIP-dG method for the Poisson equation in [GMP17].

5 Crack domain

Let Ω be the domain with a crack $(-1, 1) \times (1, 1) / ([0, 1] \times 0])$. The solution of Equation 35 is

$$u(r, \theta) = r^{1/2} \sin(\theta/2) \quad (49)$$

Numerically, ω has been set to $2\pi - \epsilon$ with $\epsilon = 10^{-3}$. The value of β must be selected within the range $(1/2, 1]$.

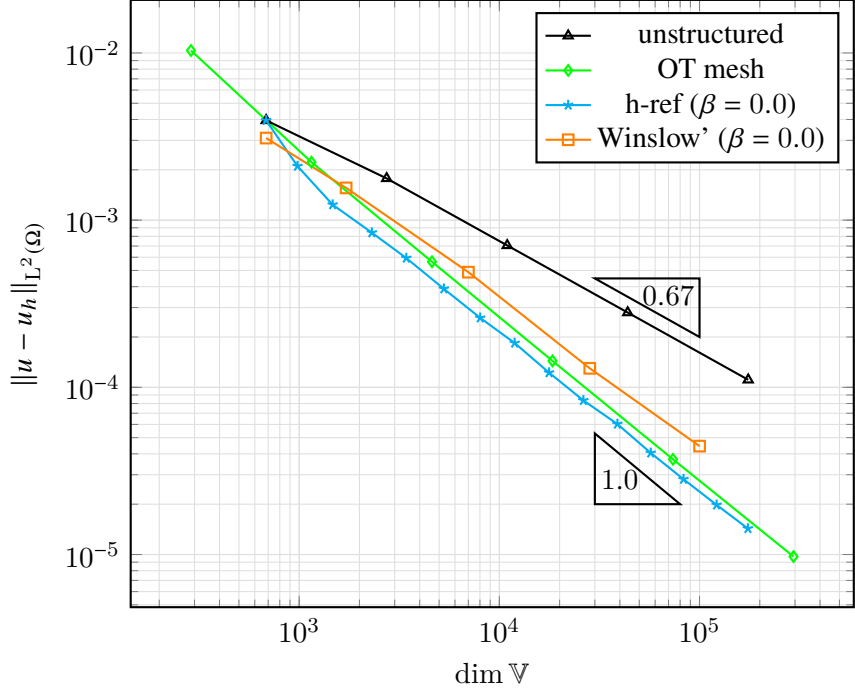
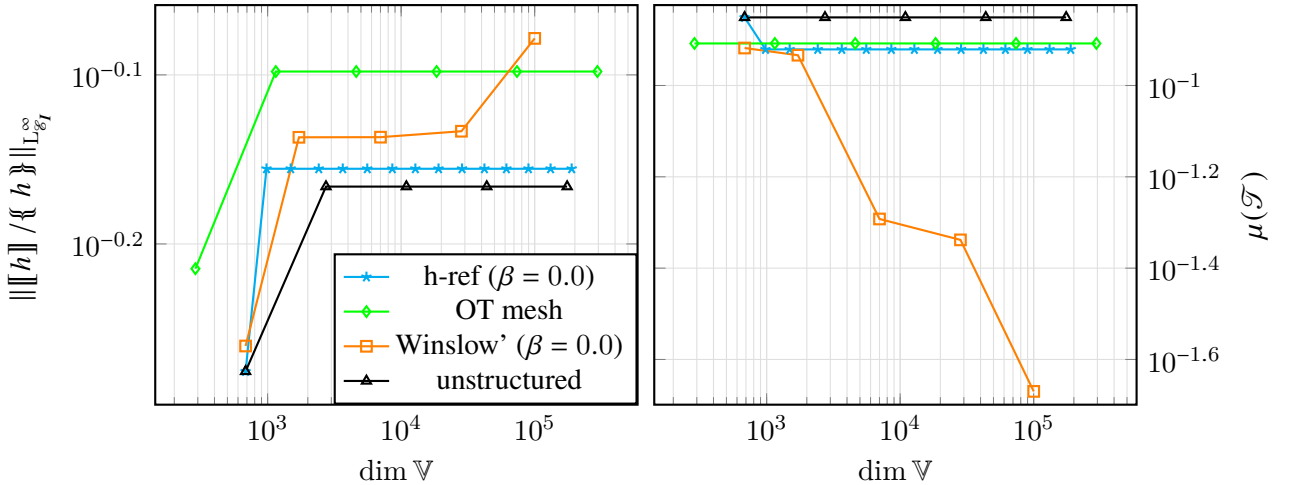


Figure 11: Asymptotic convergence rates for different adaptive mesh strategies. We observe that the OT mesh achieves the best accuracy in the family of r -adaptive methods and is almost as accurate as the ms h -refinement method.



(a) The mesh condition plotted against the dimension of the Galerkin space for different meshes.
(b) The shape regularity constant plotted against the dimension of the Galerkin space for different meshes.

Figure 12: Here we observe that the mesh condition is optimal for the h-refinement and does not depend on $\dim \mathbb{V}$. The Winslow's method performs poorly both in terms of mesh condition and shape regularity. The OT mesh condition does not depend on $\dim \mathbb{V}$ but is not optimal, as visible in Fig.10b; however the OT strategy provides highest shape regularity.

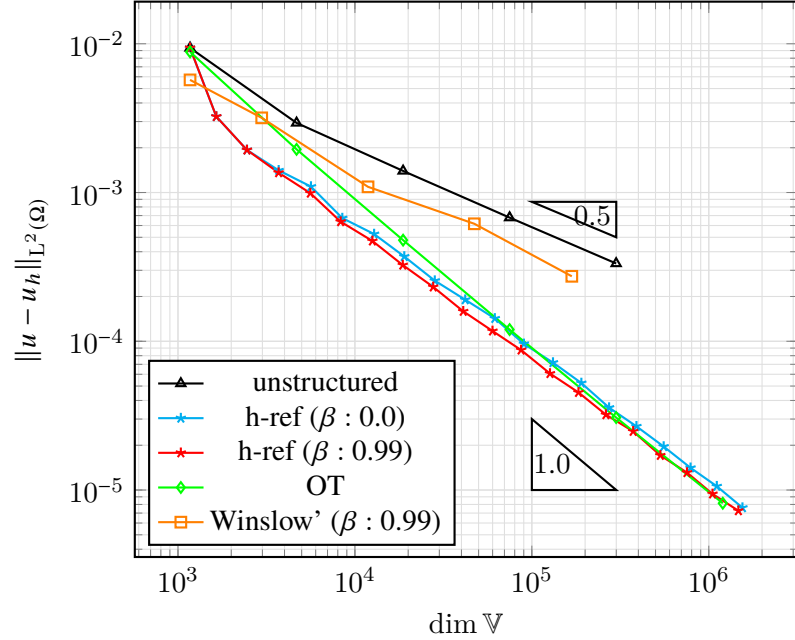
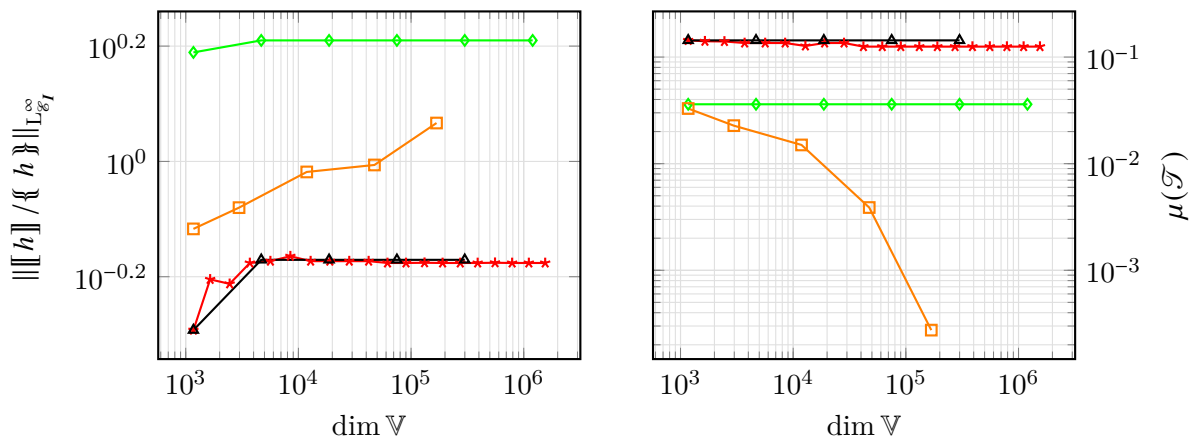
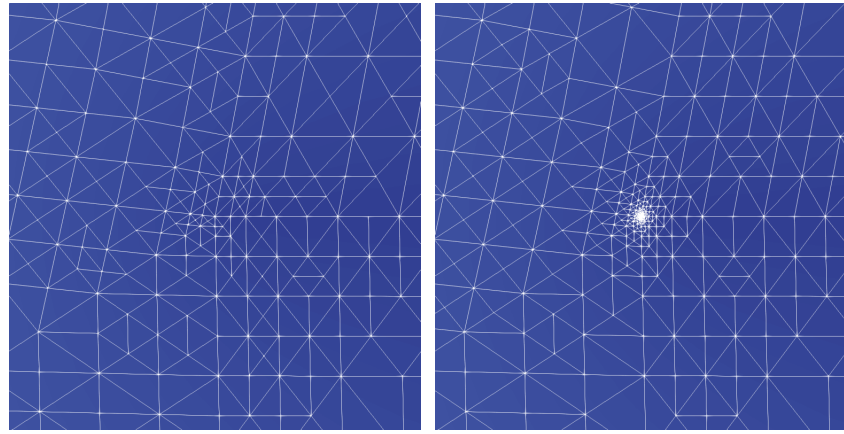


Figure 13: Asymptotic convergence rates for different adaptive strategies on \mathbb{V} . Note that the rate of convergence is optimal for h-refinement and the OT strategy. Uniform mesh refinement yields the expected convergence rate of 0.5.

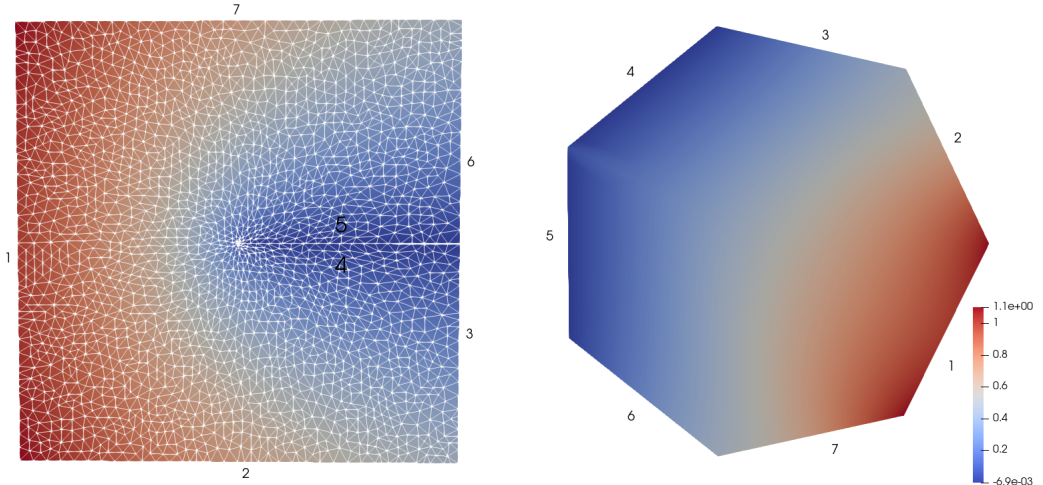


(a) The mesh condition plotted against the dimension of the Galerkin space for different meshes.

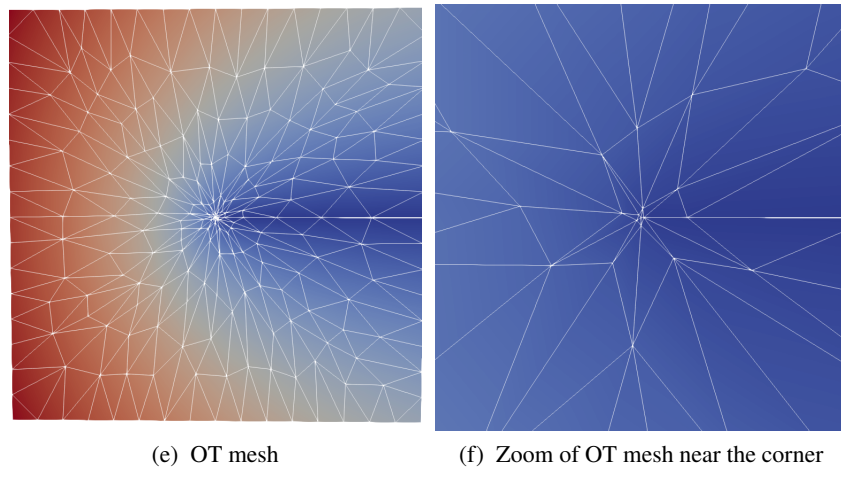
(b) The shape regularity constant plotted against the dimension of the Galerkin space for different meshes.



(a) h-refinement on re-entrant corner for $\beta = 0.0$ (b) h-refinement on re-entrant corner for $\beta = 0.99$



(c) Winslow' method with a-posteriori monitor function
 $\beta = 0.99$ (d) Computational domain for Winslow's method



(e) OT mesh

(f) Zoom of OT mesh near the corner

6 Conclusions

In this Chapter, we have analysed different adaptive mesh methods for the solution of the Poisson equation on the L-shaped domain. We first derived its SIP-dG variational form using the theoretical framework of the weighted Sobolev spaces. We stated the Theorem of existence and uniqueness of the solution, provided that a weight β is greater than a specif threshold, based on the geometry of the non-convex domain.

Our first contribution consisted in the derivation of an *a-posteriori* error upper bound for the SIP-dG method in the L^2 norm. This has enabled us to obtain a local error estimator that drives the mesh adaptation for various h - and r -adaptive strategies.

The ms h -refinement has showed optimal order of convergence independently on the parameter $\hat{\beta}$. This suggests that $\hat{\beta}$ does not directly affect β_{min} , required for the existence of the solution of the Poisson equation.

Concerning the moving mesh methods, we first conducted numerical tests using the *Winslow's* MMPDE for three different monitor functions. We observed that the a-posteriori monitor function outperforms that ones given by the gradient and curvature of the numerical solution. This should encourage the research community involved in moving mesh methods to adopt a model-dependent monitor function, provided that an a-posteriori indicator is available.

An *Optimal Transport* mesh has also been devised, inspired by the strong dependence of the solution on the radial variable near the re-entrant corner. This method is more accurate than Winslow's strategy and provides a better mesh quality. Furthermore, the computational cost is much cheaper as does not require the numerical solution of a PDE with a semi-implicit time discretisation.

Finally, we have assessed the quality of the resulting meshes in terms of *mesh condition* and *shape regularity*. While the h -refinement strategy achieves lowest mesh condition, the OT mesh provides highest shape regularity. On the contrary, the quality of the mesh generated by Winslow's method is very poor, as the mesh condition increases and the shape regularity decreases dramatically as a function of the dimension of the Galerkin space.

In conclusion, we have established that the a-posteriori estimator provides optimal order of convergence for both h - and some r -refinement strategies. The Winslow's method is not reliable as the resulting mesh becomes too skewed for increasing dofs, while the quality of the OT mesh is independent on the dimension of the Galerkin space and its accuracy is comparable to that one of h -refinement.

In the view of the above considerations, our future research directions on this topic will examine:

1. Thorough investigation on the dependence of the a-posteriori estimator with respect to the weight β , which defines the weighted Sobolev space;
2. Scalability of the algorithms through parallelisation;
3. Extension of the OT strategy by solving a Monge-Ampère type equation [BRW15];
4. The application of the h -refinement and OT strategy to other relevant time-dependent problems arising in physics, such as the Shallow-Water equations in non-convex domains.

References

- [Win66] A.M. Winslow. “Numerical solution of the quasilinear poisson equation in a nonuniform triangle mesh”. In: *Journal of Computational Physics* 1.2 (1966), pp. 149–172.
- [BR72] I. Babuška and M.B. Rosenzweig. “A Finite Element Scheme for Domains with Corners”. In: *Numer. Math.* 20.1 (1972), pp. 1–21.

- [RH73] W.H. Reed and T.R. Hill. “Triangular mesh methods for the neutron transport equation”. In: (1973).
- [BKP79] I. Babuška, R.B. Kellogg, and J. Pitkäranta. “Direct and Inverse Error Estimates for Finite Elements with Mesh Refinements”. In: *Numer. Math.* 33.4 (1979), pp. 447–471.
- [Arn82] D. Arnold. “An Interior Penalty Finite Element Method with Discontinuous Elements”. In: *SIAM Journal on Numerical Analysis* 19.4 (1982), pp. 742–760.
- [BG88] I. Babuška and B.Q. Guo. “Regularity of the Solution of Elliptic Problems with Piecewise Analytic Data. Part I. Boundary Value Problems for Linear Elliptic Equation of Second Order”. In: *SIAM Journal on Mathematical Analysis* 19.1 (1988), pp. 172–203.
- [BG89] I. Babuška and B. Q. Guo. “Regularity of the Solution of Elliptic Problems with Piecewise Analytic Data. II: The Trace Spaces and Application to the Boundary Value Problems with Nonhomogeneous Boundary Conditions”. In: *SIAM Journal on Mathematical Analysis* 20.4 (1989), pp. 763–781.
- [Dvi91] A.S. Dvinsky. “Adaptive grid generation from harmonic maps on Riemannian manifolds”. In: *Journal of Computational Physics* 95.2 (1991), pp. 450–476.
- [Ric92] G.R. Richter. “The Discontinuous Galerkin Method with Diffusion”. In: *Mathematics of Computation* 58.198 (1992), pp. 631–643.
- [CC98] B. Cockburn and S. Chi Wang. “The Local Discontinuous Galerkin Method for Time-Dependent Convection-Diffusion Systems”. In: *SIAM Journal on Numerical Analysis* 35.6 (1998), pp. 2440–2463.
- [Sch98] C. Schwab. *p-and hp-finite element methods: Theory and applications in solid and fluid mechanics*. Oxford University Press, 1998.
- [WWR99] C. Weiming, H. Weizhang, and D.R. Robert. “An r -Adaptive Finite Element Method Based upon Moving Mesh PDEs”. In: *Journal of Computational Physics* 149.2 (1999), pp. 221–244.
- [Arn+00] D. Arnold et al. “Discontinuous Galerkin Methods”. In: vol. 11. 2000, pp. 89–101.
- [CC01] B. Cockburn and S. Chi Wang. In: *Journal of Scientific Computing* 16 (2001), pp. 173–261.
- [LTZ01] R. Li, T. Tang, and P. Zhang. “Moving Mesh Methods in Multiple Dimensions Based on Harmonic Maps”. In: *Journal of Computational Physics* 170.2 (2001), pp. 562–588.
- [Arn+02] D. Arnold et al. “Unified Analysis of Discontinuous Galerkin Methods for Elliptic Problems”. In: *SIAM J. Numer. Anal.* 39 (2002).
- [ZS02] C. Zhiqiang and K. Seokchan. “A Finite Element Method Using Singular Functions for the Poisson Equation: Corner Singularities”. In: *SIAM Journal on Numerical Analysis* 39.1 (2002), pp. 286–299.
- [ZSG02] C. Zhiqiang, K. Seokchan, and W. Gyungsoo. “A finite element method using singular functions for the Poisson equation: crack singularities”. In: *Numerical Linear Algebra with Applications* 9.67 (2002), pp. 445–455.
- [Wih03] T. Wihler. “Discontinuous Galerkin FEM for elliptic problems in polygonal domains”. PhD thesis. 2003.
- [BS08] S.C. Brenner and L.R. Scott. *The Mathematical Theory of Finite Element Methods*. Vol. 15. Texts in Applied Mathematics. Springer, 2008.
- [BHR09] C. Budd, W. Huang, and R. Russell. “Adaptivity with moving grids”. In: *Acta Numerica* 18 (2009), pp. 111–241.

- [LW10] A. Logg and G.N. Wells. “DOLFIN”. In: *ACM Transactions on Mathematical Software* 37.2 (2010), pp. 1–28.
- [HR11] W. Huang and R. Russell. *Adaptive Moving Mesh Methods*. Vol. 174. 2011.
- [BRW15] C.J. Budd, R.D. Russell, and E. Walsh. “The geometry of r -adaptive meshes generated using optimal transport methods”. In: *Journal of Computational Physics* 282 (2015), pp. 113–137.
- [SH16] K. Seokchan and L. Hyung-Chun. “A finite element method for computing accurate solutions for Poisson equations with corner singularities using the stress intensity factor”. In: *Computers and Mathematics with Applications* 71.11 (2016), pp. 2330–2337.
- [GMP17] E. Georgoulis, C. Makridakis, and T. Pryer. “Babuška-Osborn techniques in discontinuous Galerkin methods: L^2 -norm error estimates for unstructured meshes”. In: *arXiv:1704.05238* (2017).
- [EG21] Alexandre Ern and Jean-Luc Guermond. *Finite Elements I: Approximation and Interpolation*. 2021.